

Load Tests on Post-Tensioned Masonry Walls

Nebojsa Mojsilovic¹ and Peter Marti²

Post-tensioning of structural masonry has been advanced by recent research and is increasingly being used for new construction as well as strengthening of existing structures [Ganz (1989, 1991), SchulPtz and Scolforo (1991)].

Within the framework of a research project on the response of masonry subjected to combined actions [Mojsilovic and Marti (1994), Mojsilovic (1995)], load tests were performed on six post-tensioned masonry walls made of calcium-silicate blocks and hollow clay bricks. This paper presents the results of these tests and comparisons with theoretical predictions considering both geometric and material nonlinearities.

TEST PROGRAM

Figure 1(a) illustrates the principle of the tests. The walls were subjected to an axial load, Q , which was kept constant while applying a moment, M_0 , at the base to produce an increasing end rotation, \mathcal{J} , in a deformation controlled manner. Figs. 1(b) and 1(c) show the cross sections of the walls and masonry units, respectively.

Test parameters and masonry properties are summarized in Table 1. Both the KH 18 blocks and the BH 18 bricks had dimensions of 180 x 250 x 135 mm (7.1 x 9.8 x 5.3 in.). The wall height, h , corresponded to one or two stories. The axial loads, Q , were selected to produce average compressive stresses of either 0.65 or 1.94 MPa (94 or 281 psi) a based on the gross cross-sectional area of the wall.

The calcium-silicate blocks contained four cylindrical holes with a diameter of 50 mm (2 in.), producing a void ratio of 18 percent. The clay bricks contained four large holes, which together with a series of smaller holes correspond to a void ratio of 41 percent. The uniaxial compressive strengths, f_b , reported in Table 1 were obtained from standard tests on the masonry units and refer to their gross cross-sectional area.

Dry, factory-made mortar was mixed with water on the test site to construct the walls. Average 28-day compressive strengths, determined from standard tests on 160 x 40 x 40 mm (6.3 x 1.6 x 1.6 in.) mortar prisms, were equal to 15.4 and 17.5 MPa (2,233 and 2,538 psi) for the calcium silicate block and the hollow clay brick masonry walls, respectively. Both bed and head joints were 10 mm (0.4 in.) thick.

Values of compressive strength, f_x , and modulus of elasticity, E_x , given in Table 1 were obtained from standard uniaxial compressive tests performed on masonry prisms according to RILEM recommendations (1981).

Test walls were built in running bond on concrete base slabs with dimensions of 200 x 1200 x 400 mm (7.9 x 47.2 x 15.7 in.) (Figure 2). Together with the similar, 300 mm (11.8 in.) thick concrete slabs at the top, the base slabs allowed proper anchorage of the monostrands using hardware developed by VSL international [Ganz (1991)]. While the base slabs contained self-activating dead-end anchor-

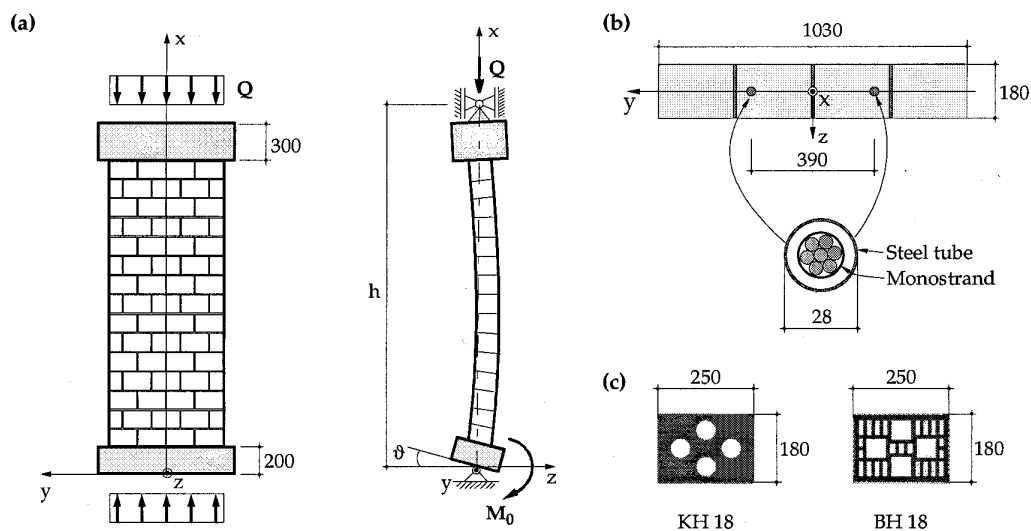


Figure 1—Geometry and notation: (a) Principle of tests; (b) Wall cross-section; (c) Masonry units. Note: all dimensions in mm

¹ Research Associate, Institute of Structural Engineering, ETH Zurich, Switzerland.

² Professor of Structural Engineering, Institute of Structural Engineering, ETH Zurich, Switzerland.

Table 1. Test Parameters and Masonry Properties (1 m = 3.28 ft, 1 kN = 224.8 lb, 1 MPa = 145 psi)

Test	K7	K8	B11	B12	B13	B14
Masonry Units	Calcium-Silicate Blocks KH18		Hollow Clay Bricks BH18			
h [m]	5.0		2.6		5.0	
Q [kN]	120	360	360	120	360	
A_{net}/A [%]	82		59			
f_b [MPa]	25.8		31.5			
f_x [MPa]	12.1		10.7			
E_x [GPa]	7.3		7.2			

ages, the top slabs were equipped with standard stressing anchorages. In order to introduce the monostrands from the top of the wall, each wall was equipped with two steel tubes passing through the holes of the masonry units. These tubes were composed of 1 m long pieces, having an outer diameter of 28 mm (1.1 in.) and a wall thickness of 1.5 mm (0.06 in.). The plastic-sheathed, 16 mm (0.6 in.) nominal diameter monostrands had a cross-sectional area of 150 mm² (0.23 in.²), a guaranteed ultimate tensile strength of 265 kN (59,572 lb), and were each prestressed to 100 kN (22,480 lb).

Figure 3 shows the test set-up. Axial load was applied by two hydraulic jacks that were anchored to the laboratory's strong floor via tension rods. The base rotation was produced by a hydraulic jack that was attached to a lateral frame which, in turn, was fixed to the base slab. A cantilever attached to the top support was used to hold the wall in place and to take the small horizontal reaction necessary for maintaining equilibrium.

Apart from applied loads, forces in monostrands and base rotations, measurements included deflections, strains on the wall surfaces and cracks widths.

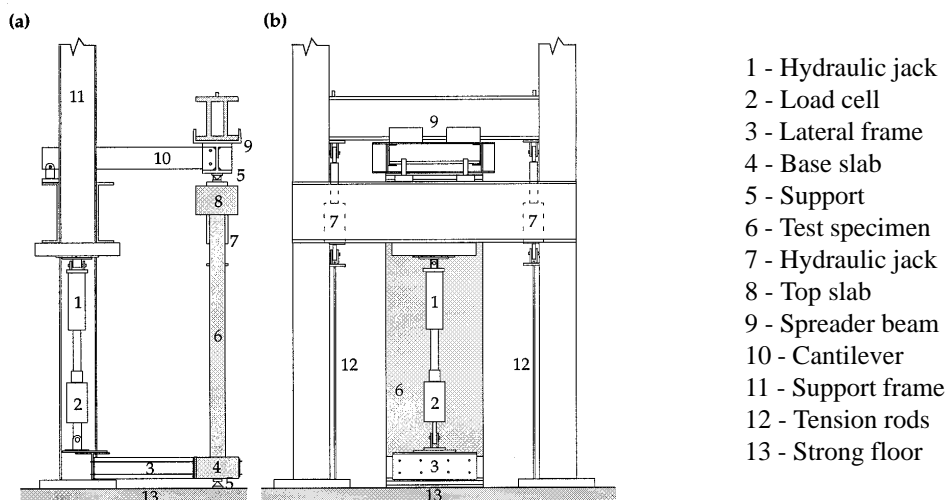


Figure 3—Test Set-up: (a) Section; (b) Elevation



Figure 2—Wall Construction

TEST RESULTS

Due to experimental inaccuracies, the axial loads varied somewhat among similar specimens. Furthermore, self weights of specimen, top slab and support, spreader beam, hydraulic jacks and tension rods added to the load applied by the jacks, so that the effective axial loads were somewhat bigger than the values of Q given in Table 1. The values of Q_{eff} reported in Figure 4, refer to the top of the base slab, i. e. $x = 200$ mm (7.9 in.) according to Figure 1(a).

Figure 4 shows the variation of base moments, M_o , and the total forces, P , in the monostrands depending on the base rotation \mathcal{J} . Larger values of Q_{eff} corresponded to larger maximum base moments, M_o , and a more brittle response. Furthermore, the increase of the forces P in the monostrands was less pronounced for the higher walls than for the shorter walls. Failure of all specimens was governed by crushing of the compression zone.

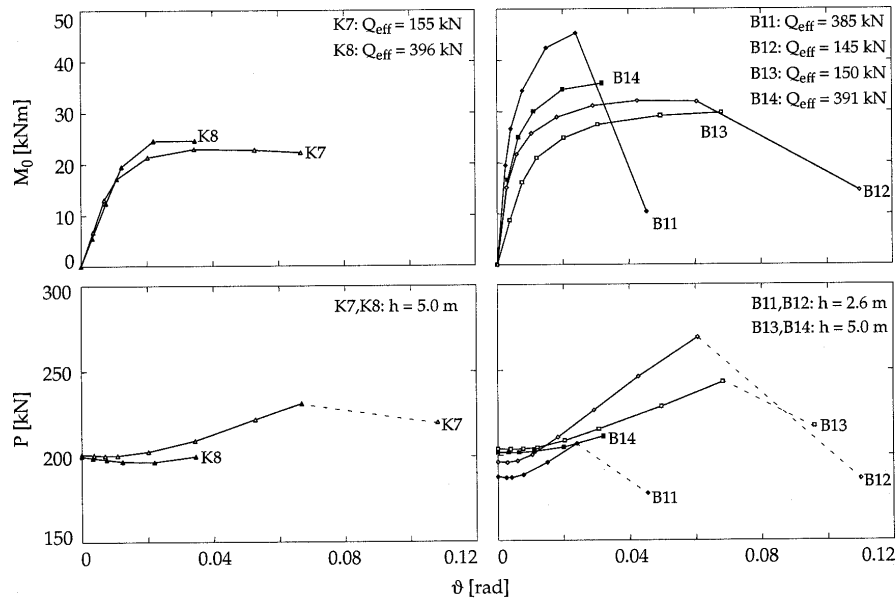


Figure 4—Variation of Base Moments and Forces in Monostrands with Increasing Base Rotation (1 kN = 224.8 lbs, 1kNm = 737 ft lbs)

Figure 5 illustrates the deformation of Specimen K7 prior to failure and Figure 6 provides a set of selected deflection profiles. Ignoring self-weight of the wall, the bending moment M at any section can be determined from known values of M_0 , Q_{eff} and w , i. e.

$$M = M_0 \left(1 - \frac{x}{h} \right) + Q_{eff} w \quad (1)$$

Thus, associating curvatures, χ , determined from strain readings on the wall surfaces, with the corresponding moments M , the moment-curvature diagrams shown in Figure 7 can be obtained.



Figure 5—Deformation of Specimen K7 Prior to Failure

Finally, Figure 8 shows the relationship between measured crack widths in bed joints, r , and associated curvatures, χ .

DISCUSSION

General Observations

Compared to non-prestressed walls, post-tensioning results in increased cracking loads and better crack distribution. Cracks were concentrated near the base of non-prestressed walls, but were well distributed over the bottom half of post-tensioned walls [Mojsilovic and Marti (1994)].

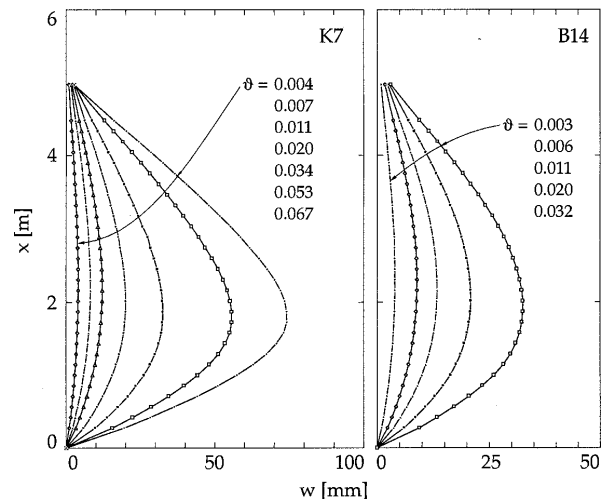


Figure 6—Selected Deflection Profiles for Specimens K7 and B14 (1mm = 0.039 in., 1m = 3.28 ft)

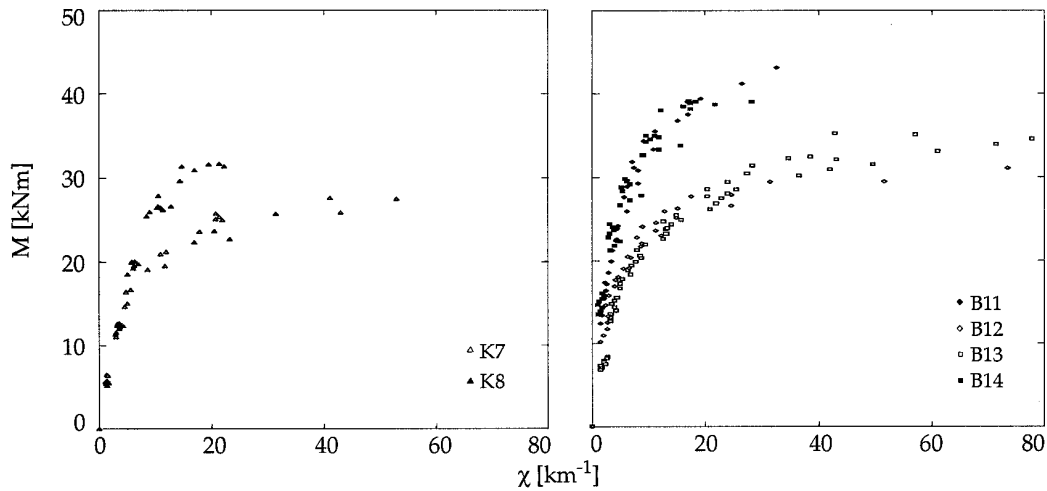


Figure 7—Moment-curvature Diagrams (1kNm = 737 ft lbs)

Post-tensioning also results in increased flexural resistance. A reasonable approximation of the ultimate flexural moment can be obtained from a simple rigid-perfectly plastic analysis according to Figure 9(a). Assuming the compression zone to be uniformly stressed to the net brick or block compressive strength, $f_{b,net} = f_b A/A_{net}$ one gets

$$M_u = (Q_{eff} + P) \left(\frac{t}{2} - \frac{Q_{eff} + P}{2f_{b,net}} \right) - e_p P \quad (2)$$

where e_p denotes the maximum possible eccentricity of the monostrand. Using actual values of Q_{eff} , P and t (180 mm (7.11 in.)), setting $e_p = 5$ mm (0.2 in.), and accounting for the values of f_b and A_{net}/A given in Table 1, Figure 9(b) compares the maximum moments recorded in the experiments with the theoretical predictions according to Equation 2. The assumption of $e_p = 5$ mm (0.2 in.) is justified by the fact that the steel tube was held in the center of the block cavities by mortar as well as by tube couplers. The relatively poor predictions for Walls K8 and B14 can be explained by the fact that no readings were taken close to failure and hence, the maximum moments recorded in these two experiments must have been exceeded considerably by the actual maximum moments.

Deflection Profiles

Assuming linearly elastic behaviour of the wall shown in Figure 10, we get

$$w = \frac{M_0}{Q_{eff}} \left\{ \frac{\sin[k(h-x)]}{\sin(kh)} + \frac{x}{h} - 1 \right\} \quad (3)$$

where

$$k = \sqrt{\frac{Q_{eff}}{EI}} < \frac{\pi}{h} \quad (4)$$

and $EI = \text{constant}$ denotes the flexural rigidity of the wall. Derivation of Equation 3 assumes that the tendon axis deflects with the wall axis, i. e. there are no relative lateral displacements between these axes and thus, the force P in the prestressing tendons does not contribute to second order effects.

The rotation $\vartheta = dw/dx$ at the base of the wall ($x = 0$) equals

$$\vartheta = \frac{M_0}{Q_{eff}} \left[\frac{1}{h} - k \cot(kh) \right] \quad (5)$$

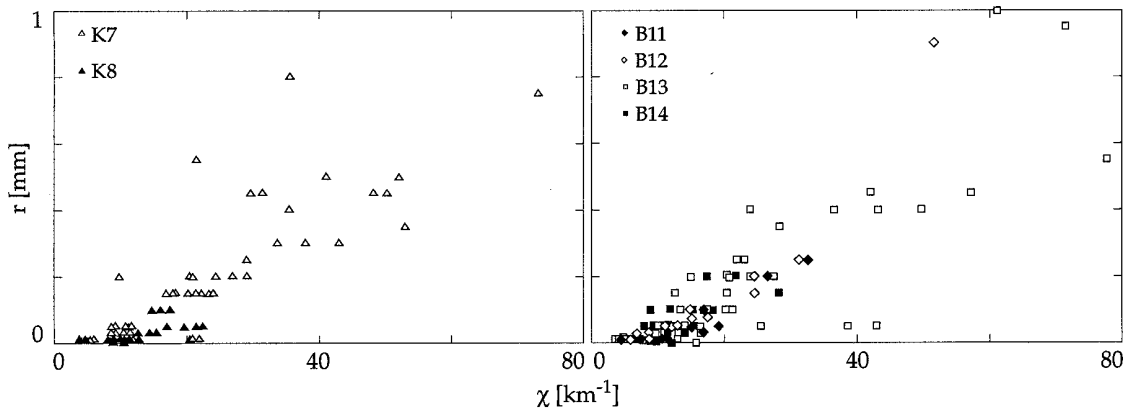


Figure 8—Crack Widths and Associated Curvatures (1mm = 0.039 in.)

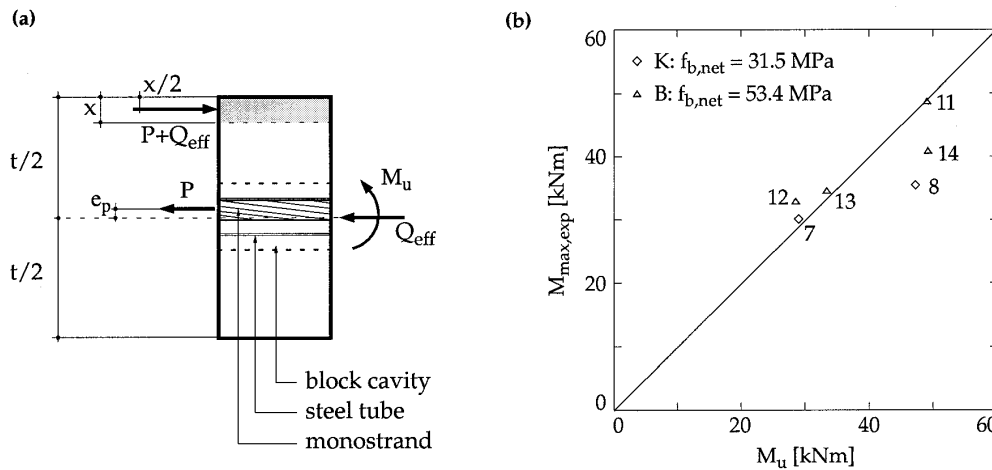


Figure 9—Ultimate Flexural Moment: (a) Internal Forces; (b) Comparison with Maximum Moments Recorded in Experiments (1 kNm = 737 ft lbs, 1 MPa = 145 psi)

and for $k < \pi / (2h)$, the eccentricity of Q_{eff} , $e = w + M_0 (1 - x/h) / Q_{eff}$, assumes the maximum M_0 / Q_{eff} at $x = 0$. Similarly, for $k > \pi / (2h)$, the maximum eccentricity occurs at $x = h - \pi / (2k)$ and equals $M_0 \sin(kh) / Q_{eff}$.

Using secant stiffnesses determined from Figure 7, application of Equation 3 leads to the theoretical deflection profiles shown in Figure 11. The experimental values are very well predicted for uncracked wall behavior, after cracking, use of the secant stiffness for the maximum moment (as a constant value of EI over the entire wall height) results in increasingly crude approximations. Based on Figure 7, a column-deflection-curve analysis (accounting for the variable EI over the wall height) could be easily performed to improve the predictions [Thürlimann and Schwartz (1987)].

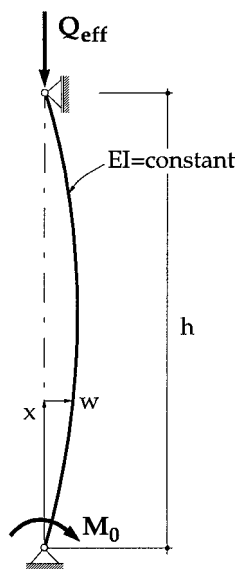


Figure 10—Linearly Elastic Wall

CONCLUSIONS

Post-tensioning enhances cracking loads, improves cracking behavior, and results in increased flexural resistance of masonry walls.

Except for possible eccentricities of the tendons relative to the (deflected) wall axis, post-tensioning forces do not contribute to instability of the wall but do contribute to the wall's flexural stiffness.

Ultimate flexural moments are well predicted by a rigid-perfectly plastic analysis using net compressive strength values of the masonry bricks or blocks.

A linearly elastic analysis accounting for second order effects and using secant stiffness values corresponding to the maximum flexural moments results in good predictions for the response of post-tensioned masonry walls well into their cracked state.

Based on the moment-curvature diagrams given in this paper, column-deflection curve analyses can be performed in cases where it is desirable to account for non-uniform stiffness distribution over the wall height.

ACKNOWLEDGMENTS

The research underlying this paper was conducted at ETH Zurich under the direction of the second author. Financial support was obtained from the Swiss Commission for Technology and Innovation and the Swiss clay-brick, calcium-silicate block and concrete block manufacturers.

REFERENCES

Ganz, H.R., "New Post-Tensioning System for Masonry," Proceedings of the 5th Canadian Masonry Symposium, Vancouver, June 1989, pp. 165-175.

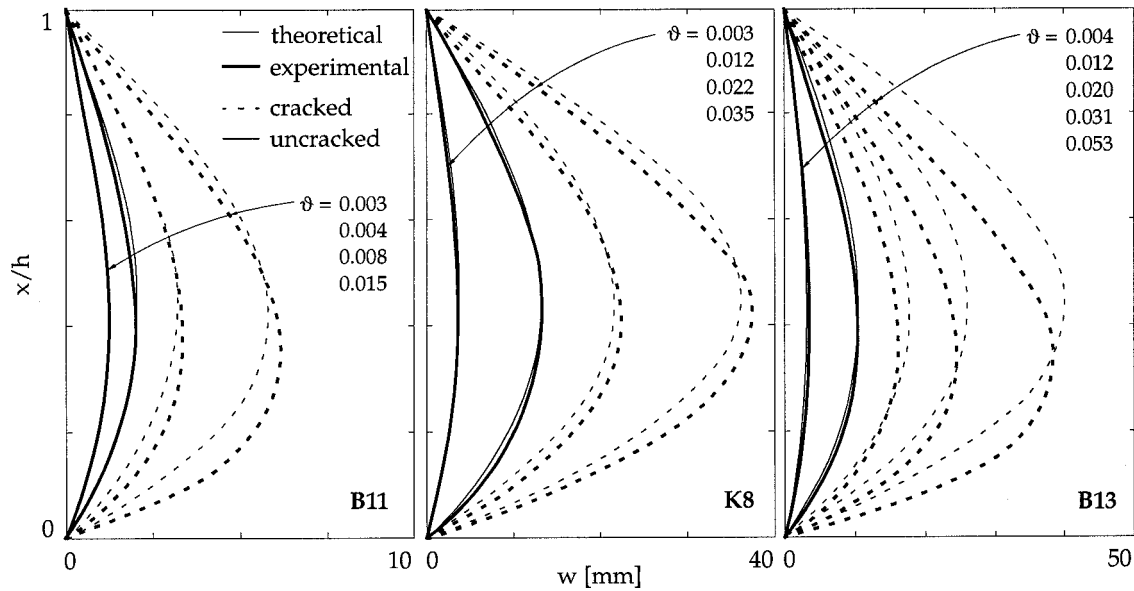


Figure 11—Comparison of Theoretical and Experimental Deflection Profiles for Three Walls (1mm = 0.039 in.)

Ganz, H.R., "Post-Tensioned Masonry Structures," VSL Report Series, No. 2, VSL International, Bern, 1991, pp. 35.

Mojsilovic, N., "On the Response of Masonry Subjected to Combined Actions (in German)," Report No. 216, Institute of Structural Engineering, ETH Zurich, Dec. 1995, pp. 136.

Mojsilovic, N., and Marti, P., "Tests on Masonry Subjected to Combined Actions (in German)," Report No. 203, Institute of Structural Engineering, ETH Zurich, April 1994, pp. 91.

RILEM, "General Recommendations for Methods of Testing Load Bearing Walls," Materials and Structures, Vol. 13, No. 78, Nov.-Dec. 1981, pp. 431-445.

Schultz, A.E., and Scolforo, M.J., "An Overview of Prestressed Masonry," The Masonry Society Journal, Vol. 10, No. 1, Aug. 1991, pp. 6-21.

Thürlimann, B., and Schwartz, J., "Design of Masonry Walls and Reinforced Concrete Columns with Column-Deflection-Curves," Proceedings, International Association for Bridge and Structural Engineering, Vol. 108, 1987, pp. 17-24.

NOTATIONS

A = gross cross-sectional area
 A_{net} = net cross-sectional area
 B = clay brick masonry
 e = eccentricity of Q_{eff}

e_0 = eccentricity of Q_{eff} at bottom support
 e_p = eccentricity of post-tensioning tendon
 E = modulus of elasticity
 E_x = modulus of elasticity determined from tests on RILEM specimens
 f_b = compressive strength of bricks or blocks
 $f_{b'net}$ = net compressive strength of bricks or blocks
 f_x = compressive strength of masonry perpendicular to bed joints
 h = wall height
 I = moment of inertia
 k = coefficient
 K = calcium-silicate block masonry
 M = flexural moment
 $M_{max\ exp}$ = maximum moment recorded in experiment
 M_0 = moment at bottom support
 M_u = theoretical ultimate moment
 P = force in post-tensioning tendons
 Q = axial load
 Q_{eff} = effective axial load at top of base slab
 r = crack width
 t = wall thickness
 w = deflection
 x = coordinate, compression zone thickness
 y = coordinate
 z = coordinate
 χ = curvature
 J = rotation at bottom support